Chemical Science

ROYAL SOCIETY OF CHEMISTRY

PERSPECTIVE

View Article Online
View Journal | View Issue

Cite this: *Chem. Sci.*, 2021, **12**, 2368

All publication charges for this article have been paid for by the Royal Society of Chemistry

Received 28th September 2020
Accepted 6th December 2020

DOI: 10.1039/d0sc05363e

rsc.li/chemical-science

Controlling ultrasmall gold nanoparticles with atomic precision

Nan Xia[ab] and Zhikun Wu *[ab]

Gold nanoparticles are probably the nanoparticles that have been best studied for the longest time due to their stability, physicochemical properties and applications. Controlling gold nanoparticles with atomic precision is of significance for subsequent research on their structures, properties and applications, which is a dream that has been pursued for many years since ruby gold was first obtained by Faraday in 1857. Fortunately, this dream has recently been partially realized for some ultrasmall gold nanoparticles (nanoclusters). However, rationally designing and synthesizing gold nanoparticles with atomic precision are still distant goals, and this challenge might rely primarily on rich atomically precise gold nanoparticle libraries and the in-depth understanding of metal nanoparticle chemistry. Herein, we review general synthesis strategies and some facile synthesis methods, with an emphasis on the controlling parameters determined from well-documented results, which might have important implications for future nanoparticle synthesis with atomic precision and facilitate related research and applications.

1. Introduction

Gold is a noble element with chemical inertness and enduring physical qualities, even after exposure to extreme conditions for tens or hundreds of years. Long after the discovery of gold in Bulgaria five thousand years ago, ancient Egypt and China started using colloidal gold for therapeutic and decorative purposes around the 5th or 4th century B.C.[1–3] The scientific realization of such colloidal gold can be traced back to Michael Faraday's research in 1857 when he successfully prepared a ruby-red gold colloid through the reduction method.[4] After a great deal of experimental and theoretical research was performed in the following 150 years, gold colloids (gold nanoparticles) were found to not only be beautiful but also to exhibit rich properties such as optics, sensing, catalysis, and biomedicine properties.[1–3,5–7]

The properties of gold nanoparticles are often related to a set of physical parameters that may include the size, shape, composition, and structure.[8,9] Over the past few decades, extensive efforts have been devoted to modulating gold nanoparticles to control their morphologies and compositions. Despite narrow dispersion in continuously improved synthesis, gold nanoparticles are still not atomically precise due to their polydisperse sizes and indefinable surface architecture. Controlling gold nanoparticles with atomic precision can be of great utility not only in tuning their properties accurately but also in obtaining an atomic-level understanding of their structure–property correlations (*e.g.* structure–catalytic activity relationships[10]). It has long been a major dream of nanochemists to prepare atomically precise gold nanoparticles, which was realized by the emergence of gold nanoclusters.

Gold nanoclusters (Au NCs), or ultrasmall gold nanoparticles, are aggregates of certain gold atoms protected by ligands with precise molecular formulae. Au NCs can be rigorously categorized as a branch of the broader class of gold nanoparticles and provide an ideal platform for the pursuit of atomically precise control of gold nanoparticles. In comparison with previously studied gold nanoparticles, Au NCs exhibit intriguing properties, such as discrete electronic energy levels, quantized charging, intrinsic chirality, strong luminescence, and excellent catalytic selectivity.[11–13] The architecture of Au NCs usually consists of various numbers of metal atoms, types of metal atoms and ligands, surface bonding (staples), packing styles of metal atoms, *etc.* Thus, unique molecular-like structures and properties render Au NCs sensitive to one or a few atomic alterations and accessible for control by methods such as chemists modifying organic molecules through various synthetic methods.[14–18] Nevertheless, rationally designing and synthesizing Au NCs are still challenging due to the limitation of synthesis methods and NC chemistry understanding.

This review aims to provide a comprehensive summary of the recent progress in precisely controlling Au NCs at the atomic level based on some existing synthesis methods, mainly including gold salt (complex) reduction, ligand induction, and antigalvanic reduction, among others. We will highlight the controlling parameters of how to influence the structures and properties of the resulting Au NCs. Finally, we conclude by

[a]*Key Laboratory of Materials Physics, Anhui Key Laboratory of Nanomaterials and Nanostructures, Institute of Solid State Physics, Chinese Academy of Sciences, Hefei 230031, P. R. China. E-mail: zkwu@issp.ac.cn*

[b]*Institute of Physical Science and Information Technology, Anhui University, Hefei 230601, P. R. China*

presenting our perspective and suggestions for the further development of controlling Au NCs with atomic precision.

2. Synthesis strategy

Understanding the fundamentals of the underlying reaction process is extremely important to control Au NCs with atomic precision, which has attracted extensive attention in recent years. For example, Hainfeld *et al.* reported the preparation of size-controllable gold nanoparticles (2–6 nm) by tuning the polymeric Au(I) thiolate precursor size with pH control.[19] Subsequently, Jin *et al.* achieved the controllable synthesis of NCs by tuning the kinetics of the formation of Au(I):SR intermediates, leading to the formation of Au_{25} NCs with high yield.[20] They found that Au(I):SR intermediates formed at 0 °C, which, under very slow stirring conditions, were distributed in a narrow range of 100–400 nm, whereas those obtained at room temperature had a multimodal distribution with a broader range of 1–10 000 nm. Soon afterwards, an important process – "size focusing"‘ – was revealed in the growth of Au_{25} by Jin and coworkers.[21,22] This aging stage involves a slow conversion process of the initially formed mixture of differently sized Au_n clusters into uniform Au_{25}. Then, motivated by the formation of Au_{19} NCs using a weak reducing agent (borane *tert*-butylamine complex) instead of the strong reducing $NaBH_4$ agent, Wu and Jin proposed a general strategy for the synthesis of Au NCs, involving kinetic control and thermodynamic selection processes (Scheme 1),[23] which can be detailed as (i) the kinetic control of the initial size distribution of crude NCs by controlling the reduction speed, the ratio of Au : SR, and other parameters; and (ii) thermodynamic selection (or size focusing) during the aging process by controlling the aging time, temperature, and other parameters, leading to robust (thermodynamically favorable) cluster species. Xie *et al.* also demonstrated such a strategy in the synthesis of water-soluble Au_{25} in aqueous solution by using electrospray ionization mass spectrometry (ESI-MS) to monitor the reaction process. They adopted the NaOH-mediated $NaBH_4$ reduction method to tune the formation kinetics of Au NCs and accelerate the thermodynamic selection of Au_{25}.[24] Another work by them is the usage of CO as a reducing agent that kinetically controls crude clusters, and Au_{25} NCs were also obtained after thermodynamically controlled size focusing.[25] Although various synthetic methods have been developed in the last decade, the formation of atomically precise (narrow-sized) Au NCs can be mainly illustrated by kinetic control and thermodynamic selection (not limited to the gold salt (complex) reduction method (*vide infra*)).

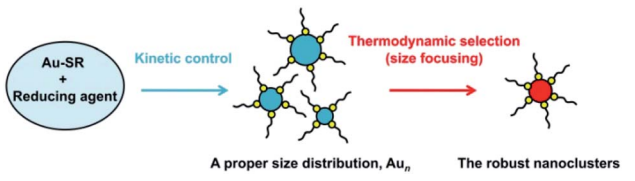

Scheme 1 Illustration of the synthesis strategy "kinetic control and thermodynamic selection" for atomically monodisperse gold nanoclusters.

3. Synthesis method and controlling factors

There are two basic routes used for synthesizing atomically precise gold nanoparticles in terms of the charge state of the starting gold (Scheme 2): one route is the reduction of gold salt (complex), and the other is the transformation of gold nanoparticles (including nanoclusters).[18,26–28] For the first route, the synthesis method can be dubbed the "gold salt (complex) reduction method"; for the second route, there are two major synthesis methods, including the ligand induction method and anti-galvanic reduction method, in terms of inducing reagents. Below, we will specifically review the synthesis method and controlling parameters.

3.1 Gold salt (complex) reduction method and controlling parameters

The gold salt (complex) reduction method is also known as a one-pot synthesis, and is one of the most versatile and best studied synthetic methods. This method is usually referred to as the direct reduction of a mixture of gold salt (complex) and other reactants, leading to final nanoparticles after essential purification but without any further disposal. The first gold colloid was synthesized by Faraday in 1857 from the aqueous reduction of gold chloride by phosphorus.[4] An important advancement of this method was developed by Brust *et al.* (the Brust–Schiffrin method) in 1994.[29] They exploited thiols for gold nanoparticle synthesis *via* a two-phase system in which gold chloride was transferred in toluene using a phase-transfer reagent. Following the footsteps of Brust *et al.*, many groups, including Whetten, Murray, Tsukuda, Jin and other groups, conducted tremendous research on the synthesis of gold thiolate nanoparticles and nanoclusters. Gold salt (complex) reduction (often modified from the Brust–Schiffrin method) has been an efficient approach used to control the synthesis of Au NCs. The controlling parameters comprise the ligand, temperature, solvent, and others.

3.1.1 Ligands. Ligands influence not only kinetics but also thermodynamics. Different ligands would lead to Au NCs with various sizes and structures due to the differences between their

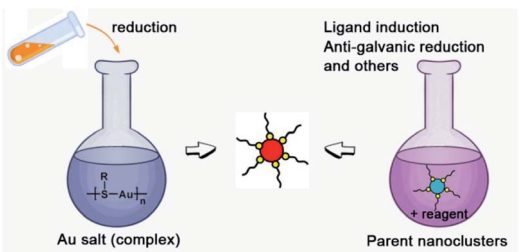

Scheme 2 Schematic illustration of the synthesis route classification in terms of the charge state of the starting gold.

steric hindrance, electronic structure, bonding style and so on. Many Au NCs protected by different ligands, including thiols, phosphines, alkynes and mixed ligands, have been synthesized and structurally determined in recent years. Taking thiols an example, Au_{18},[30] Au_{23},[31] Au_{25},[32,33] Au_{30},[34] Au_{42},[35] Au_{102},[36] and Au_{144} (ref. 37 and 38) were obtained by using cyclohexanethiol, phenylethanethiol, adamantanethiol, 4-*tert*-butylbenzenelthiol, *p*-mercaptobenzoic acid, and phenylmethanethiol, respectively. Fig. 1 lists a few typical Au NCs protected by different ligands.[30–46]

Generally, smaller NCs are formed when using ligands with stronger steric repulsion, which can explain why the reported NCs protected by cyclohexanethiol, adamantanethiol and phosphines are often smaller than those protected by phenylethanethiol, 4-*tert*-butylbenzenelthiol and so on;[30,31,34,36–38] Phosphine ligands (containing several benzene rings) often give rise to the formation of rod-shaped packing,[41,44,45] and conjugated thiophenols or alkynes favor the formation of NCs with FCC structures,[11] for example, most of the 4-*tert*-butylbenzenelthiolated gold nanoclusters obtained by reduction of gold salt (complex) are fcc-structured such as $Au_{36}(TBBT)_{24}$,[47,48] $Au_{44}(TBBT)_{28}$,[47,48] $Au_{52}(TBBT)_{32}$,[49] $Au_{56}(TBBT)_{34}$,[50] and $Au_{92}(TBBT)_{44}$ [51] (TBBT: 4-*tert*-butylbenzenelthiolate), while the phenylethanethiolated gold nanoclusters synthesized by reduction of gold salt (complex) generally adopt core–shell structures such as $Au_{25}(PET)_{18}$,[32,33] $Au_{38}(PET)_{24}$ [37] and $Au_{144}(PET)_{60}$ [38] except for $Au_{52}(PET)_{32}$ [52] (PET: phenylethanethiolate).

The ligand type not only influences the atomic packing mode, but also affects structure distortion. For example, on the basis of density functional theory calculations of a series of $[Au_{25}(SR)_{18}]^-$ nanoclusters, Tlahuice-Flores *et al.* revealed that low-polarity R groups do not disturb the $Au_{25}S_{18}$ framework greatly, while in the case of *p*-thiolphenolate ligands (*p*-SPhX), a remarkable distortion of the $Au_{25}S_{18}$ framework destroys the inversion symmetry, the distortion increasing in the given order X = H, Cl, NO_2 and CO_2H. Similarly, the *N*-acetyl-cysteine ligand also notably distorts the framework.[53]

3.1.2 Temperature. Temperature also influences reaction kinetics and thermodynamics. Among the early studies on Au_{25}, Jin *et al.* found that the products obtained at 0 °C showed characteristic absorption bands of Au_{25} at 670, 450, and 400 nm.[20] However, a major product of larger Au clusters (Au∼140) was formed at room temperature. The state of the Au(I):SR aggregates was proven to account for such control *via* dynamic light scattering measurements. Regarding the synthesis of water-soluble Au_{25} protected by mercaptohexanoic acid, Xie *et al.* reported that 40 °C is the optimal temperature to synthesize Au_{25} in aqueous solution, while overheating (such as at 60 °C) induced the transformation of Au_{25} into mixed clusters in the reaction.[54] Li *et al.* found that the high temperature treatment (60 °C) largely decreased the reaction time compared with the low temperature (0 °C) case used for synthesizing Au_{25} NCs protected by glutathione.[55]

3.1.3 Solvent. Solvents have a great impact on the aggregation of Au complex precursors and the dispersion of intermediate NCs in the reaction; thus, solvents were used for the selective control of the product clusters. $Au_{25}(PET)_{18}$ can be facilely prepared in tetrahydrofuran (THF).[21] When the solvent was changed to methanol, the major product was proven to be $Au_{144}(PET)_{60}$,[56] the structure of which was recently revealed by using benzyl mercaptan as a ligand under similar conditions. Wu *et al.* reported the synthesis of a novel $Au_{38}(PET)_{26}$ (Au_{38T}) cluster in dichloromethane (Fig. 2).[57] Au_{38T} and the previously reported Au_{38Q} are structural isomers with the same formula but different atomic architectures (Fig. 2). The biicosahedral Au_{23} core in Au_{38Q} is composed of two fused Au_{13} icosahedra by sharing a Au_3 face, while the Au_{23} core in Au_{38T} can be viewed as one Au_{12} cap and one Au_{13} icosahedron (Fig. 2A(a)) fused together by sharing two Au atoms. The surface staples of these two Au_{38} isomers are also different from each other. More significantly, Au_{38T} exhibits remarkably higher catalytic activity

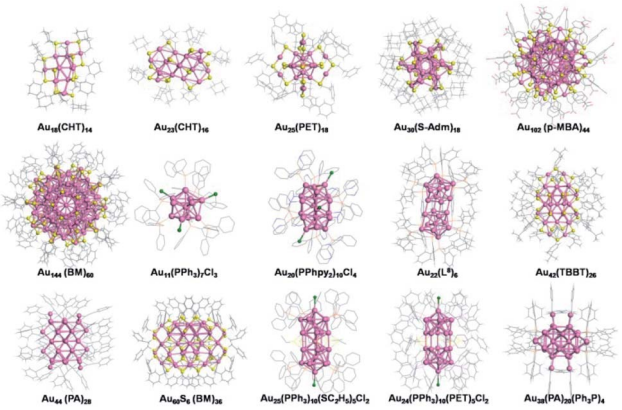

Fig. 1 Representative crystal structures of Au NCs capped by different ligands using the gold salt (complex) reduction method. CHT-H: cyclohexanethiol; PET-H: phenylethanethiol; H-S-Adm: adamantanethiol; *p*-MBA-H: *p*-mercaptobenzoic acid; BM-H: benzyl mercaptan; PPh_3: triphenylphosphine; $PPhpy_2$: bis(2-pyridyl)-phenylphosphine; L^8: 1,8-bis(diphenylphosphino) octane; TBBT-H: 4-*tert*-butylbenzenelthiol; PA: phenylacetylene; H-SC_2H_5: ethanethiol.

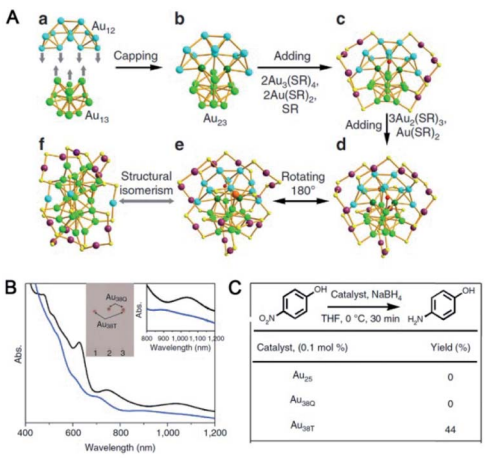

Fig. 2 (A) Structures of Au_{38T} (blue) and Au_{38Q} (black). (B) UV-vis spectra of Au_{38T} and Au_{38Q} in toluene. (C) Catalytic activities of Au_{25}, Au_{38T} and Au_{38Q} (reproduced from ref. 57 with permission from Springer Nature, Copyright (2015)).

than Au_{38Q} at low temperatures (for example, at 0 °C) in the 4-nitrophenol reduction reaction, indicating the structure–property correlation in Au NCs (Fig. 2C).

Note that, except for the kinetic influence, solvents also have a thermodynamic influence on the reaction, since solvents provide the environment and influence the stability of the reaction species.

3.1.4 Reducing reagent. Based on the abovementioned synthesis strategy, kinetic control, such as the control of reduction kinetics, is quite important for governing the size of Au NCs. The widely used $NaBH_4$-reduction-based synthesis offers fast reaction kinetics and might lead to a relatively broad size distribution of intermediate Au_x (the ligands were omitted for clarification). Weak reducing agents are thus expected to slow down the reduction kinetics and finally produce different NCs. For example, $Au_{19}(PET)_{13}$ was obtained using a borane *tert*-butylamine complex as the reducing agent,[23] while Au_{25} was often formed in this reaction system after $NaBH_4$ reduction. Carbon monoxide (CO) is a mild gaseous reducing agent that was also introduced in the synthesis of Au NCs by Xie and coworkers. As shown in Fig. 3A, they reported a versatile method to tailor the size of thiolated Au NCs by simple CO reduction as well as tuning the solution pH value.[58] A red-emitting $Au_{22}(SG)_{18}$ NC was also synthesized by this method (Fig. 3B).[59] The bright luminescence (QY ~8%) of Au_{22} at ~665 nm was proposed to originate from long Au(I)-thiolate motifs *via* the aggregation-induced emission pathway. Pradeep *et al.* reported the synthesis of a highly fluorescent and biocompatible $Au_{18}(SG)_{14}$ NC using sodium cyanoborohydride ($NaBH_3CN$), a mild and selective reducing agent.[60] Antoine *et al.* synthesized Au_{25} isomers using three isomers of mercaptobenzoic acids (*p*/*m*/*o*-MBA) as capping ligands by slow reduction of Me_3NBH.[61]

Except for the type of reducing agent, the amount of the reducing agent could be considered for the control synthesis of gold nanoclusters.[62,63] For example, Xie *et al.* investigated the synthesis process of water-soluble Au_{25} by using a stoichiometric amount of $NaBH_4$. Due to the precise control of reducing electrons from $NaBH_4$, a series of intermediate clusters (Au_4–Au_{29}) were confirmed with the help of the real-time mass spectrometry technique. Such stoichiometric[62] or sub-stoichiometric[63] controls on the amount of the reducing agent not only enrich the library of gold nanoclusters, but also largely contribute to the mechanistic understanding of the reaction.

3.1.5 Assistant reagent. In addition to the selection of reducing agents, the addition of assistant reagents to the reaction, such as acids, bases, foreign metal ions, *etc.*, was also proven to influence reaction kinetics and thermodynamics. For example, Xie *et al.* reported a NaOH-assisted reduction method for synthesizing mono-, bi, and tri-thiolate protected Au_{25} with good capability and high yield.[24] The addition of NaOH can not only reduce the reduction ability of $NaBH_4$ by retarding the hydrolysis of $NaBH_4$ but can also accelerate the etching ability of free thiolate ligands. During the synthesis of Au NCs by CO reduction, the size of the obtained NCs increased with increasing pH.[58]

Recently, the Wu group developed an acid-induction method *via* the addition of common acids (such as nitric acid, hydrochloric acid and acetic acid).[52] Hydrogen ions that detached from the acid can accelerate the hydrolysis of $NaBH_4$ and strengthen the reactivity of $NaBH_4$. Meanwhile, they can interact with thiol groups, thus weakening the interaction between Au and thiolate and reducing the etching ability of thiolate. The influences of protons on the reaction kinetics and thermodynamics might be contrary to those of OH^- reported by Xie *et al.*[24] A novel $Au_{52}(PET)_{32}$ NC, whose kernel structure was revealed to be the isomer of the kernel structure of $Au_{52}(TBBT)_{32}$, was synthesized *via* this method. As shown in Fig. 4A–H, the gold atom fcc packing in $Au_{52}(PET)_{32}$ is a quadrangular prism-like core with defective top and bottom facets. The two defective facets consist of 6 gold atoms instead of 12 gold atoms for a complete facet. In $Au_{52}(TBBT)_{32}$, the 48-gold kernel comprises 4 × 4 × 6 Au atom layers along the *X*-, *Y*-, and *Z*-axes, respectively, and each layer has 8 gold atoms. The comparison of the UV/vis/NIR spectra indicated that such isomerization greatly influenced the electronic structure of the two Au_{52} NCs (Fig. 4I).

When adding acetic acid in the synthesis of Au NCs protected by TBBT, $Au_{42}(TBBT)_{26}$ instead of $Au_{36}(TBBT)_{24}$ and $Au_{44}(TBBT)_{28}$ formed after aging for two hours.[35] The Au_{34} kernel of $Au_{42}(TBBT)_{26}$ is composed of four cuboctahedra, which is identical to that of $Au_{44}(TBBT)_{28}$. Of note, the surface staples are totally different between these two clusters. In $Au_{42}(TBBT)_{26}$, the bridging thiolates and dimeric staples anchor the [100] facets, and each of the monomer staples anchor each [110] facet, with no staples anchoring the [111] facet. However, in $Au_{44}(TBBT)_{28}$, the [100], [111] and [110] facets are protected

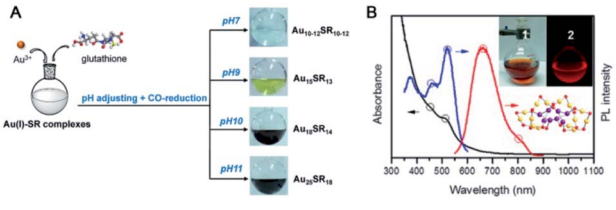

Fig. 3 (A) The synthesis of differently sized Au NCs using the CO-reduction method by adjusting pH. (B) UV-vis absorption and fluorescence spectra of $Au_{22}(SG)_{18}$ (reproduced from ref. 58 and 59 with permission from the American Chemical Society, Copyright (2013, 2014)).

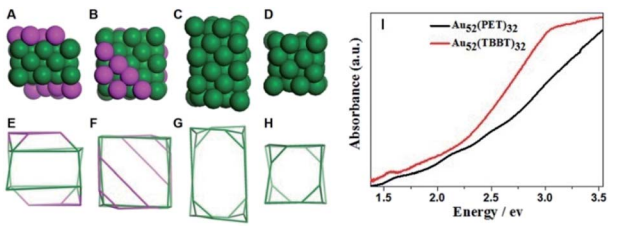

Fig. 4 (A and E) The Au_{50} kernel of $Au_{52}(PET)_{32}$ with defective facets; (C and G) Au_{48} kernel of $Au_{52}(TBBT)_{32}$; (B, D, F, and H) aerial view of (A), (C), (E), and (G); (I) photon-energy plot of $Au_{52}(PET)_{32}$ and $Au_{52}(TBBT)_{32}$.

by bridging thiolates, a dimeric staple and monomeric staple, respectively. The clusters only exist with different staple styles and share the same kernel and ligands, which are termed homoligand–homokernel–heterostaple clusters. Moreover, the reduction of the two Au–SR units led to decreased stability of $Au_{42}(TBBT)_{26}$ compared with that of $Au_{44}(TBBT)_{28}$ and a decrease in photoluminescence.

Later, $Au_{44}(TBBT)_{26}$ and $Au_{48}(TBBT)_{28}$ were prepared *via* the acid-induction method.[64] These two nanoclusters and $Au_{38}(PET)_{26}$ can be regarded as kernel homologues due to their similar kernel structures: one identical Au_{23} only differs in its number of capping gold atoms: 0, 6, and 8 (see Fig. 5). It is found by DFT calculations that the HOMOs-LUMOs are mainly distributed on the Au_{23} unit for every nanocluster, and the electrochemical properties of the three clusters are similar, both indicating that the Au_{23} unit acts as a "functional group". In this work, the concepts of homologue, homology and functional groups were introduced into nanochemistry to help understand the structure–property relationship for the first time.

Another assistant reagent is foreign metal ions. The co-reduction of Au and other metal ions would produce alloy NC intermediates and, finally, monometallic cluster products. For example, a non-fcc-structured $Au_{42}(TBBT)_{26}$ (Au_{42N}) nanocluster was successfully synthesized in the presence of cadmium ions by Wu and coworkers.[65] The addition of Cd may influence kinetics and thermodynamics in the production of Au_{42N} nanoclusters by, for example, forming unstable Au/Cd intermediates, tuning the reducing ability of $NaBH_4$, or influencing the etching rate of thiol. Au_{42N} is the structural isomer of abovementioned $Au_{42}(TBBT)_{26}$ (Au_{42F}) with an fcc packing kernel produced in the acid-induction method. As shown in Fig. 6, Au_{42N} contains a non-fcc Au_{26} kernel that can be split into three parts consisting of 9, 9, and 8 Au atoms. The Au_{26} kernel is capped by several motifs, including four $Au_3(TBBT)_4$, four $Au(TBBT)_2$ and two TBBT units. Wu *et al.* found that the photoluminescence emission of Au_{42F} was approximately twice as extensive as that of Au_{42N}, indicating that the fcc structure does not actually inhibit the emission compared with the non-fcc structure, which was further demonstrated by DFT calculations.

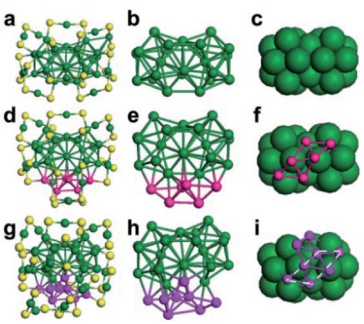

Fig. 5 Comparison of the kernel structures of $Au_{38}(PET)_{24}$, $Au_{44}(TBBT)_{26}$ and $Au_{48}(TBBT)_{28}$ (reproduced from ref. 64 with permission from John Wiley and Sons, Copyright (2018)).

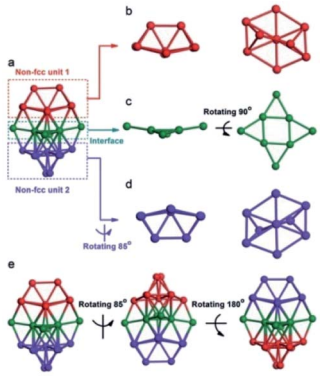

Fig. 6 The kernel structure of Au_{42N} (reproduced from ref. 65 with permission from John Wiley and Sons, Copyright (2019)).

3.1.6 Others. Synthesis protocols also influence the size of the as-obtained NCs. For example, the stirring speed and the addition style of the reducing agent have been identified to be important for the selective synthesis of Au NCs.[66,67] The slow stirring and slow addition of $NaBH_4$ are favored by the formation of the series of Au_{20}, Au_{24}, and $Au_{39/40}$ NCs instead of Au_{25}.

3.2 Ligand induction method and controlling parameters

In early work, the ligand induction method typically involved the partial exchange of ligands for the functionalization and tailoring of the surface properties of nanoparticles, but changes in the nanoparticle size are often neglected due to the lack of structural determination.[68,69] Since the accessible structure of Au NCs was developed, great advances in ligand induction methods have been made mainly by Jin, Tsukuda, *etc.*[70,71] They introduced thermal conditions and the addition of a large excess of thiol into this method to control the size and structure of Au NCs. As one of the most important methods for synthesizing NCs, ligand induction often includes several step ligand exchange, structural transformation and size-focusing on the basis of the stability of differently sized NCs. Here, the precursor nanoclusters are not limited to monodispersed NCs and can be extended to mixed-sized NCs.

3.2.1 Ligands. Different ligands can lead to various products. In 2013, Jin *et al.* reported transformation from $Au_{38}(PET)_{24}$ to $Au_{36}(TBBT)_{24}$ by ligand induction and studied the reaction kinetics to unravel the total transformation process (see Fig. 7).[72] The inner core of Au_{36} is a truncated tetrahedral fcc Au_{28} structure, which is quite different from the biicosahedral Au_{23} core of Au_{38}. When using benzyl mercaptan as the incoming ligand, the parent Au_{38} was transformed into a novel $Au_{60}S_6(SCH_2Ph)_{36}$ ($Au_{60}S_6$) NC.[43] It consists of an fcc Au_{20} kernel and a pair of giant $Au_{20}S_3(SCH_2Ph)_{18}$ staple motifs, which are the largest staple motifs ever found in thiolated gold nanoclusters (Fig. 8A). More interestingly, $Au_{60}S_6$ NCs adopt a very special stacking sequence of 'ABCDEF' along the close-packed [001] direction with 60° rotation between two neighboring clusters (Fig. 8B). The new crystallographic stacking was named the 6H left-handed helical (6HLH) arrangement, and the fourth packing mode was revealed long after the third closest

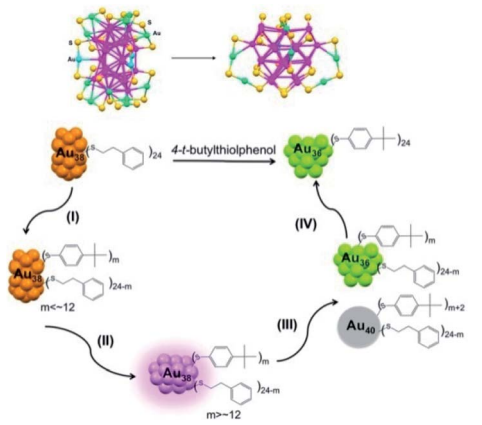

Fig. 7 Reaction pathway for the conversion of $Au_{38}(PET)_{24}$ to Au_{36}(-TBBT)$_{24}$ (reproduced from ref. 72 with permission from the American Chemical Society, Copyright (2013)).

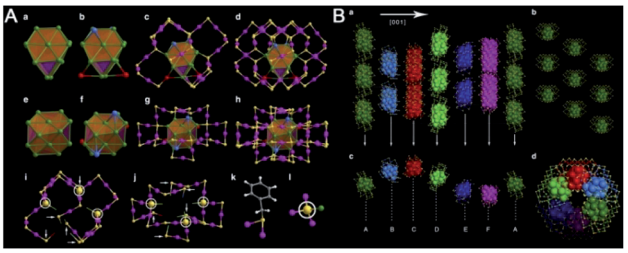

Fig. 8 (A) Anatomy of the atomic structure and (B) crystallographic arrangement of the $Au_{60}S_6$ nanocluster (reproduced from ref. 43 with permission from Springer Nature, Copyright (2015)).

crystallographic packing (4H) was discovered in 1979. The fluorescence emission intensity of such crystallized $Au_{60}S_6$ was weaker than that of amorphous $Au_{60}S_6$, indicating possible energy transfer among the 6HLH arranged structures.

Another example is the ligand exchange of $Au_{25}(PET)_{18}$. $Au_{28}(TBBT)_{20}$ nanoclusters can be synthesized by reacting Au_{25} with excess TBBT thiol.[73] As shown in Fig. 9A, $Au_{28}(TBBT)_{20}$ is chiral and can be viewed as an fcc Au_{20} kernel capped by four $Au_2(SR)_3$ dimeric staples and eight SR bridging thiolates. The Au_{20} kernel is composed of two fused cuboctahedra sharing six common atoms. The $Au_{24}(SCH_2Ph)_{20}$ nanocluster was obtained after mixing Au_{25} with benzyl mercaptan.[74] Au_{24} consists of a bitetrahedral Au_8 kernel with an fcc-based antiprismatic shape and four $Au_4(SR)_5$ tetrameric staples (Fig. 9B). More significantly, the strong fluorescence of Au_{24} NCs was rationally attributed to their particular structures compared with some other common nanoclusters. The interlocked $Au_4(SR)_5$ staples reduce emission loss by vibration, and the fully thiolate-bound kernel style strengthens electron transfer from the thiolates to the kernel through the Au–S bonds, thus leading to enhanced fluorescence.

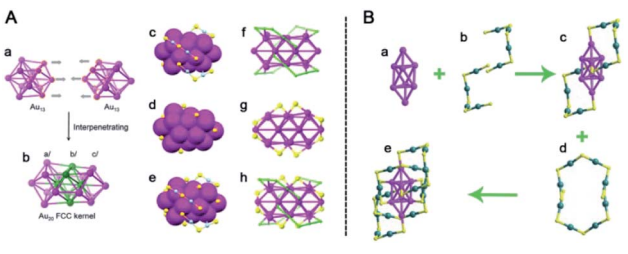

Fig. 9 (A) The Au_{20} kernel structure (a and b) and the thiolate-binding modes (c–h) in Au_{28}; (B) analysis of the $Au_{24}(SCH_2Ph)_{20}$ nanocluster structure (reproduced from ref. 73 with permission from the American Chemical Society, Copyright (2013) and ref. 74 with permission from John Wiley and Sons, Copyright (2016)).

Dass reported the synthesis of $Au_{99}(SPh)_{42}$ nanoclusters by etching $Au_{144}(PET)_{60}$ with benzenethiol.[75] They found the instability of Au_{144} upon reaction with aromatic ligands, indicating that Au NCs protected by aromatic ligands favored different cores from those protected by aliphatic ligands. However, Jin and coworkers found that $Au_{144}(PET)_{60}$ converted to $Au_{133}(TBBT)_{52}$ after treatment with excess 4-*tert*-butylbenzenethiol at 80 °C for 4 days.[76] Au_{133} has a four-shell structure. The central atom and the first shell form a 13-atom icosahedron that is wrapped by a 42-atom icosahedral shell, generating 55-atom Mackay icosahedra (MI). The third 52-atom shell is a transition layer between the Au_{55} MI and the outermost protecting layer. The resultant Au_{107} kernel is quasi-spherical and further protected by 26 monomeric staples. Notably, the surface gold-thiolate staples exhibit a self-organized helical "stripe" pattern. There are four such stripes that are bound with a curved surface clockwise or anticlockwise in the two chiral isomers.

An interesting study on the ligand effect was reported by Jin and coworkers in 2015.[77] They explored the control of the magic sizes of Au NCs by the subtle structural change of the surface protecting ligands. After etching the polydispersed Au_n clusters with isomeric methylbenzenethiols (MBT), $Au_{130}(p\text{-MBT})_{50}$ (Au_{130}), $Au_{104}(m\text{-MBT})_{41}$ (Au_{104}) and $Au_{40}(o\text{-MBT})_{24}$ (Au_{40}) NCs are obtained using *para*-, *meta*- and *ortho*-methylbenzenethiol, respectively (Fig. 10). This work revealed that the magic size and stability of Au NCs were sensitive to the surface protecting thiols. Later, the structural determination of Au_{130} and Au_{40} was also achieved.[78,79] Au_{130} is constructed in a four-shell manner with a barrel shape, while Au_{40} exhibits a Kekulé-like ring shape composed of a series of four-atom tetrahedral units.

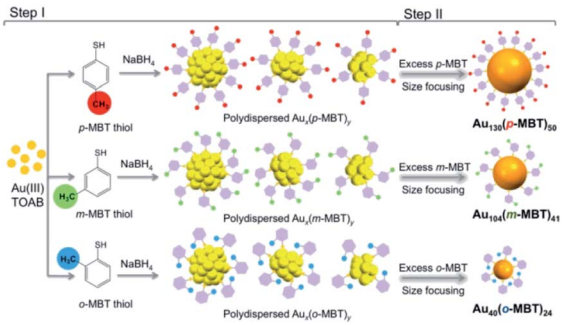

Fig. 10 The synthesis of differently magic-sized nanoclusters capped by three isomeric thiol ligands: *p*-MBT, *m*-MBT, and *o*-MBT (reproduced from ref. 77 with permission from the American Chemical Society, Copyright (2015)).

3.2.2 Temperature. The temperature used in the ligand induction method is crucial for the thermodynamic selection of the stable size of Au NCs under specific conditions. For example, Jin and coworkers successfully synthesized Au_{44}(TBBT)$_{28}$ (Au_{44}) and Au_{52}(TBBT)$_{32}$ (Au_{52}) by reacting mixed-sized Au_x(TBBT)$_y$ clusters with excess TBBT thiol at 60 °C and 80 °C, respectively. From the structures of these two NCs as well as those of Au_{28}(TBBT)$_{20}$ (Au_{28}) and Au_{36}(TBBT)$_{24}$ (Au_{36}), Jin *et al.* found periodicities in the formula, growth pattern, and property evolution of Au NCs.[47] A unified formula of Au_{8n+4}(TBBT)$_{4n+8}$ (n = 3–6) is defined, and the four clusters all adopt a kernel evolution pattern with double-stranded growth at the bottom. Wu *et al.* obtained a novel Au_{92}(TBBT)$_{44}$ (Au_{92}) nanocluster while keeping the etching process at 65 °C.[51] Au_{92} is composed of an fcc-Au_{84} kernel capped by an exterior shell including 28 TBBT thiolates and 8 Au(TBBT)$_2$ staples. Au_{92} might be a transition-sized nanoparticle bridging the non-fcc-structured and fcc-structured gold nanoclusters. Interestingly, they found a linear relationship between the major maximum absorption wavelengths and the number of gold atoms in a series of TBBT-protected Au NCs (*e.g.*, Au_{28}, Au_{36}, Au_{44}, Au_{52} and Au_{92}). They used an extrapolation method to propose that a nanocluster with ~155 gold atoms and an fcc structure may exhibit a typical surface plasmon resonance peak at ~520 nm. Recently, the synthesis and structure of Au_{56}(TBBT)$_{34}$ were reported by Wu and coworkers through etching at 50 °C.[50] Compared with the six layers of the fcc Au_{48} kernel in Au_{52}(TBBT)$_{32}$, the kernel atoms are packed in a similar manner, only with a defective layer, which is the seventh layer and consists of only 4 gold atoms (see Fig. 11A). In the same work, they found the size effect and the kernel-layer number odevity effect in both the polarity and photoluminescence of the series of TBBT-protected Au NCs. In detail, Au_{36} and Au_{52} with even number-layered kernels show weaker polarity and a higher emission intensity than those with odd number-layered kernels (*e.g.*, Au_{28}, Au_{44}, and Au_{56}). When the odevity of the layer number is fixed, the NCs with large sizes exhibit stronger polarity and weaker emission intensity than those with small sizes (Fig. 11B and C).

3.2.3 Etching time. With increasing the etching time, stable NCs with magic sizes were mainly formed during thermodynamic selection; thus, some novel NCs with low stability might be prepared by tuning the etching time. For example, in the synthesis of 2,4-dimethylbenzenethiolate (2,4-DMBT)-protected Au NCs reported by Wu's group, Au_{44}(2,4-DMBT)$_{26}$ was obtained after treating the precursors of the multisized Au_x(2,4-DMBT)$_y$ clusters with excess DMBT-H thiol at 40 °C for 20 h.[80] The Au_{44}(2,4-DMBT)$_{26}$ structure comprises a Au_{29} kernel and a surface protecting shell including two 2,4-DMBT thiolates, three Au(2,4-DMBT)$_2$, and six Au_2(2,4-DMBT)$_3$ staples (see Fig. 12A). The Au_{29} kernel of Au_{44}(2,4-DMBT)$_{26}$ is composed of face-fused biicosahedral Au_{23}, as reported in Au_{38Q}, and a special Au_6 bottom cap. Au_{44}(2,4-DMBT)$_{26}$ bears an 18-electron shell closure structure, but it is less thermostable than Au_{44}(TBBT)$_{28}$, indicating that multiple factors contribute to the thermostability of Au NCs. Later, they found that a novel Au_{49}(2,4-DMBT)$_{27}$ nanocluster was formed when the etching time was reduced to 18 h.[81] As shown in Fig. 12B, the Au_{34} kernel of Au_{49} is the combination of one non-fcc Au_{13} unit and one quasi-fcc Au_{21} unit despite some distortions. The exterior shell consists of six Au_2(2,4-DMBT)$_3$ dimers, three Au(2,4-DMBT)$_2$ monomers and three 2,4-DMBT ligands. The total structure of Au_{49} is quite different from the Au_{44}(2,4-DMBT)$_{26}$ structure mentioned above. Wu *et al.* also investigated the influence of the kernel-packing mode on the electrochemical gap (EG) using DPV and found that the fcc-kerneled gold nanocluster has a larger EG than the investigated non-fcc-kerneled nanoclusters. The EG of Au_{49} with mixed-packed kernels falls between that of the abovementioned two structures.

3.2.4 Others. Other parameters have also been explored in ligand induction methods; for example, the ratio of the thiol to the precursor might influence the attachment of the incoming ligands to the parent clusters, the extra catalyst might promote structural transformation, *etc.* After treating the precursors with 20 equivalents and 5 equivalents of cyclohexanethiol (CHT-H) at 40 °C, Wu and coworkers successfully synthesized Au_{34}(CHT)$_{22}$ and Au_{42}(CHT)$_{26}$, respectively.[82] Au_{34} can be viewed as a Au_{20} kernel or six equivalent tetrahedral Au_4 units entangled together along two helixes, further capped by three Au_3(SR)$_4$ trimer staples and five Au(SR)$_2$ monomer staples. The structure of Au_{42} consists of 8 tetrahedral units (Au_{26}) assembled along two helixes that are protected by six Au_2(SR)$_3$ dimer staples and four Au(SR)$_2$ monomer staples. Based on the resolved structures of Au_{28}(CHT)$_{20}$, Au_{34}(CHT)$_{22}$ and Au_{42}(CHT)$_{26}$, a novel kernel evolution pattern was demonstrated and depicted as alternate single-stranded growth at both ends (Fig. 13), which is remarkably different from the reported double-stranded growth at the bottom of the TBBT protected NC series.[47] Note that, compared with the one-dimensional growth mode, a two-dimensional one was recently proposed by Xu, *et al.*;[83] for the

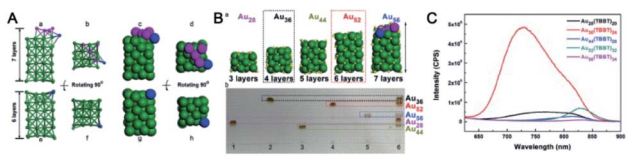

Fig. 11 (A) The comparison of the kernels of Au_{56}(TBBT)$_{34}$ and Au_{52}(TBBT)$_{32}$; (B) structure evolution (a) and thin-layer chromatography (b); (C) the photoluminescence spectra of Au_{28}(TBBT)$_{20}$, Au_{36}(TBBT)$_{24}$, Au_{44}(TBBT)$_{28}$, Au_{52}(TBBT)$_{32}$, and Au_{56}(TBBT)$_{34}$ (reproduced from ref. 50 with permission from John Wiley and Sons, Copyright (2020)).

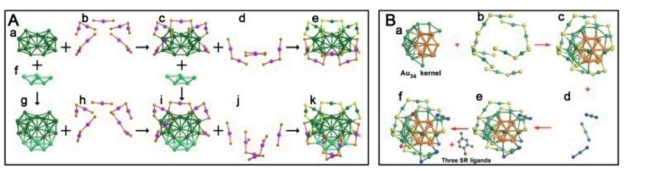

Fig. 12 (A) Anatomy of the structures of Au_{38Q} and Au_{44}(2,4-DMBT)$_{26}$ nanoclusters; (B) anatomy of the structure of the Au_{49}(2,4-DMBT)$_{27}$ nanocluster (reproduced from ref. 81 with permission from John Wiley and Sons, Copyright (2017)).

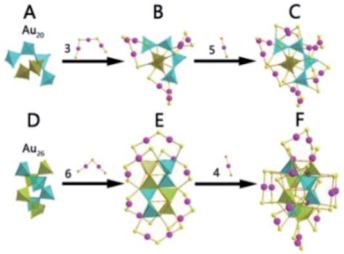

Fig. 13 The kernel, total structure and growth mode of $Au_{28}(CHT)_{20}$, $Au_{34}(CHT)_{22}$ and $Au_{42}(CHT)_{26}$.

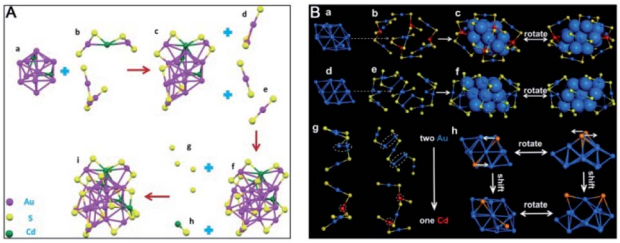

Fig. 14 Anatomy of the structure of (A) $Au_{20}Cd_4(SH)(SR)_{19}$ and (B) $Au_{26}Cd_4(CHT)_{22}$ nanoclusters (reproduced from ref. 92 with permission from John Wiley and Sons, Copyright (2018) and ref. 93 with permission from the American Chemical Society, Copyright (2019)).

building block study, various polyhedral approaches have been proposed, see ref. 84–87. In 2016, Wu *et al.* reported an interesting phenomenon: ~3 nm nanoparticles greatly promoted the transformation from Au_{44} to Au_{36} in the presence of TBBT thiol, whereas the transformation is extremely slow, even at higher temperatures without the existence of ~3 nm nanoparticles.[48] The possible mechanism is that ~3 nm particles can rivet Au_{44} on the surface and activate the staple motif of Au_{44} for subsequent attack by TBBT-H thiol.

3.3 Anti-galvanic reduction (AGR) method and controlling parameters

Anti-galvanic reduction (AGR), which was first proposed in 2012 by Wu,[88] involves the reduction of metal ions by less reactive (more noble) metals, which is the opposite of the famous GR discovered by Italian scientist Luigi Galvani. The driving force of AGR is that the oxidation potential of ultrasmall metal NPs greatly decreases to a potential that is even lower than the reduction potential of some less noble metal ions. AGR has been used for metal ion sensing, antioxidation, synthesis of atomically precise alloy NCs or monometal NCs, *etc.* For more information, readers are recommended to read a recent review article, ref. 89. In this section, we mainly focus on the controlling parameters in the AGR synthesis method.

3.3.1 Gold nanocluster precursors. Gold nanocluster precursors are the main reactants in the reaction and thus certainly play a crucial role in AGR. It is revealed that not only the precursor size but also the ligand on the nanocluster surface influence product types. For example, Wu *et al.* demonstrated that PET-protected Au_{25} can react with silver ions to produce several AuAg alloy NCs (such as $Au_{24}Ag_1(PET)_{18}$, $Au_{23}Ag_2(PET)_{18}$ and $Au_{25}Ag_2(PET)_{18}$), while glutathiolated Au_{25} generated different products when it was reacted with the same type ions.[90,91] Wu and coworkers investigated the AGR of Au_{23} and Au_{34} that were both capped by CHT thiol and obtained different products after reacting with cadmium salts: $Au_{20}Cd_4(SH)(SR)_{19}$ for Au_{23} and $Au_{26}Cd_4(CHT)_{22}$ for Au_{34}.[92,93] $Au_{20}Cd_4(SH)(SR)_{19}$ is composed of a $Au_{11}Cd_2$ kernel protected by two nonequivalent trimeric staples, one dimeric staple, two monomeric staples, four plain bridging thiolates, and one CdSH unit (Fig. 14A). The icosahedral $Au_{11}Cd_2$ kernel is distorted due to the introduction of two Cd atoms. Surprisingly, a unique CdSH motif has been observed for the first time in NCs, and this doping style was also different from previously reported modes. $Au_{26}Cd_4(CHT)_{22}$ can be viewed as a distorted face-centered cubic (fcc) Au_{16} kernel capped by two "paw-like" $Cd(S–Au–S)_3$ staples, one pentameric $Au_3Cd_2(SR)_8$ staple and one monomer $Au(SR)_2$ staple (Fig. 14B). Compared to the structure of Au_{34}, the doping of four Cd atoms not only changed the surface structure but also induced a distinct distortion of the gold kernel.

Recently, Zhu *et al.* carefully investigated the Ag doping position of TBBT-protected Au_{28} and Au_{36} NCs by reacting with the Ag(I)SR complex.[94] Compared with the general doping of Ag atoms in the isotropic nanocluster (*e.g.*, $Au_{25}(SR)_{18}$), only specific Au atoms of Au_{28} and Au_{36} (*e.g.*, Au atoms at the vertex sites in the metal core or in the staples) can be replaced by Ag atoms, which was attributed to the electrophilic effect revealed by DFT calculations.

3.3.2 Ion precursor. The type of ion precursor was extensively revealed to influence both AGR kinetics and thermodynamics. In 2015, Wu *et al.* studied the doping of $Au_{25}(PET)_{18}$ with different Ag(I) precursors, including Ag–EDTA, Ag–PET and Ag–DTZ complexes (EDTA: ethylenediamine tetraacetic acid disodium salt; DTZ: dithizone), which have different chelation abilities to Ag ions.[91] They used mass spectrometry and preparative thin-layer chromatography (PTLC) and observed different products for different Ag precursors, such as $Au_{25}(PET)_{18}^0$, $Au_{24}Ag_1(PET)_{18}$, $Au_{23}Ag_2(PET)_{18}$, and $Au_{25}Ag_2(PET)_{18}$. However, Au_{25} was transformed into $Au_{44}(PET)_{32}$ when it was reacted with copper ions, and $Au_{44}(SC_2H_4Ph)_{32}$ exhibited the highest catalytic activity among the investigated nanoclusters for the reduction of nitrophenol at low temperatures.[95] Another example is the Cd doping of $Au_{25}(PET)_{18}$: $Au_{24}Cd(PET)_{18}$ ($Au_{24}Cd$) and $[Au_{13}Cd_2(PPh_3)_6(PET)_6(NO_3)_2]_2Cd(NO_3)_4$ ($Au_{26}Cd_5$) formed when the Cd–PET complex and $Cd(PPh_3)_2(NO_3)_2$ were used as the ion precursor, respectively.[96–98] The Cd atom replaced one Au atom of Au_{25} in the former reaction, while the two Cd atoms capped on Au_{25} with six dimer staples lost in the latter case (see Fig. 15). $Au_{24}Cd$ can further react with Hg^{2+} to form $Au_{24}Hg(PET)_{18}$, and the doping of Cd or Hg in Au_{25} can effectively tune the electronic structure of the parent Au_{25}. The doping of Cd can also greatly improve the parent nanocluster's catalytic activity; for example, the doped product $Au_{26}Cd_5$ exhibits high activity and substrate tolerance as well as good recyclability in catalyzing the A^3-coupling reaction. In addition, the AGR product is ion dose dependent as well.[91] For example, in the reaction of $Au_{25}(PET)_{18}$

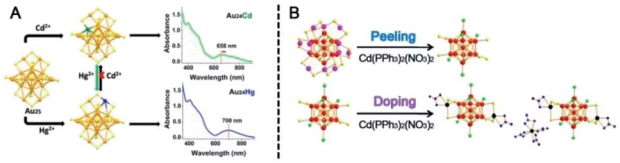

Fig. 15 (A) The doping position and UV-vis spectra of $Au_{24}Cd$ and $Au_{24}Hg$. (B) Structural evolution from Au_{25} to $Au_{26}Cd_5$ (reproduced from ref. 97 with permission from the American Chemical Society, Copyright (2019) ref. 98 with permission from John Wiley and Sons, Copyright (2017)).

with Ag–DTZ, as the Ag–DTZ dose increases, the content of $Au_{24}Ag(PET)_{18}$ in the product mixture increases while the content of $Au_{25}Ag_2(PET)_{18}$ decreases and is finally negligible when the Ag : Au atomic ratio reaches 2 : 1.

When a special ion precursor–Au complex is introduced to react with Au NCs (such reactions were dubbed quasi- or pseudo-AGR), the parent NCs will convert into others by adding or losing Au atoms. Wu *et al.* found that fluorescent $Au_{24}(PET)_{20}$ was easily synthesized by reacting Au_{25} with the Au–PET complex and revealed that the electrochemical gap was enlarged with decreasing size.[99] Very recently, the same group reported the simultaneous synthesis of two $Au_{28}(CHT)_{20}$ isomers by mixing $Au_{23}(CHT)_{16}$ with the Au–CHT complex.[100] The two isomers, consisting of the same $Au_{20}(CHT)_8$ kernel and different outer staples, can reversibly transform into each other through dissolution and crystallization processes with oscillating fluorescence. Wu *et al.* also revealed a module replacement (MR)-like process during the pseudo-AGR of $Au_{48}(CHT)_{26}$.[101] The MR-like process involves the replacement of the local structural unit (including three or more Au atoms) by a new one. As-obtained $Au_{37}(CHT)_{23}$ and $Au_{48}(CHT)_{26}$ share the same $Au_{31}(CHT)_{12}$ section as the other section ($Au_6(CHT)_{11}$ *vs.* $Au_{17}(CHT)_{14}$). $Au_{37}(CHT)_{23}$ exhibited stronger photoluminescence but weaker photothermy than $Au_{48}(CHT)_{26}$, indicating that photoluminescence and photothermy are balanced and can be at least partly converted into each other.

3.3.3 Phase number. AGR is initially performed in one phase by directly mixing the parent nanoclusters with foreign metal salts or complexes. Very recently, the Wu group designed a two-phase AGR method that consisted of $Au_{44}(TBBT)_{28}$ and TBBT thiol in an organic solvent and cadmium ions in aqueous solution, leading to the production of novel $Au_{47}Cd_2(TBBT)_{31}$ alloy nanoclusters, while only Au_{36} was obtained in a common one-phase system.[102] The introduction of the water phase may cause weakened interactions between Cd^{2+} and Au_{44}, the reduced oxidation ability of Cd^{2+}, and the decreased etching ability of thiols, which influence reaction kinetics and thermodynamics and lead to different products. $Au_{47}Cd_2(TBBT)_{31}$ is composed of a Au_{29} kernel and a protective shell that includes the following staple motifs: two paw-like $Cd(S–Au–S)_3$, three $Au_2(TBBT)_3$, one $Au_3(TBBT)_4$, and three $Au(TBBT)_2$ staples (Fig. 16B). As shown in Fig. 16A, the center of the Au_{29} kernel is a Au_{10} unit, which can be viewed as an Archimedean anti-prism capped with two half-octahedra. Two Au_9 units cap the front of

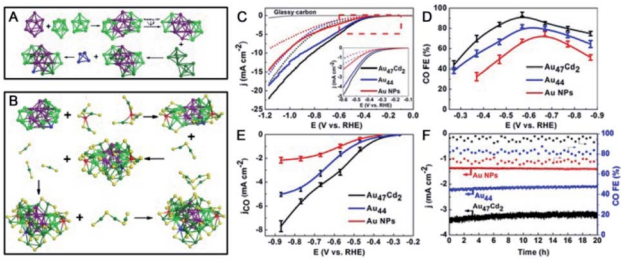

Fig. 16 (A) Kernel structure and (B) anatomy of the structure of $Au_{47}Cd_2(TBBT)_{31}$. (C) LSV curves of $Au_{47}Cd_2(TBBT)_{31}$, $Au_{44}(TBBT)_{28}$ and the *ca.* 1.5 nm Au NPs in an Ar-saturated (dotted line) and a CO_2-saturated (full line) 0.5 M $KHCO_3$ solution. (D) CO faradaic efficiency of the catalysts examined with different applied potentials. (E) The corresponding CO partial current density. (F) The stability test (reproduced from ref. 102 with permission from John Wiley and Sons, Copyright (2020)).

the Au_{10} unit by sharing two Au_3 facets. Another two octahedra cap the back of Au_{10} by sharing two Au_3 facets, and a Au_4 tetrahedron is connected to the bottom of Au_{10} by sharing one Au_3 facet. Notably, $Au_{47}Cd_2$ has higher faradaic efficiencies for electrocatalytically reducing CO_2 to CO (96% at −0.57 V) than the parent Au_{44} NC (Fig. 16C–F).

3.3.4 Others. The choice of solvent can also affect the NC product in AGR. Taking the reaction of $Au_{25}(PET)_{18}$ with Ag^+ as an example, polydisperse $Au_{24-x}Ag_x(PET)_{18}$ NCs were obtained in dichloromethane or toluene, whereas dominant $Au_{25}Ag_2(PET)_{18}$ was produced in acetonitrile.[103] The two introduced Ag atoms do not replace the Au atoms in $Au_{25}(PET)_{18}$ but simply deposit on $Au_{25}(PET)_{18}$, as revealed by UV/vis/NIR spectra, mass spectra, and theoretical calculations (Fig. 17). Moreover, $Au_{25}Ag_2(PET)_{18}$ exhibited an enhanced catalytic activity in the hydrolysis of 1,3-diphenylprop-2-ynyl acetate.

Since trimetallic nanoclusters can be achieved by successive AGR reactions, the sequence of the usage of metal complexes also affects the product type. For example, $Au_{25}(PET)_{18}$ first reacted with Hg^{2+} ions and then with the Ag(I)–PET complex, leading to the formation of $Au_{16.8}Ag_{7.2}Hg_1(PET)_{18}$ nanoclusters.[104] When the sequence of Hg^{2+} ions and the Ag(I)-PET

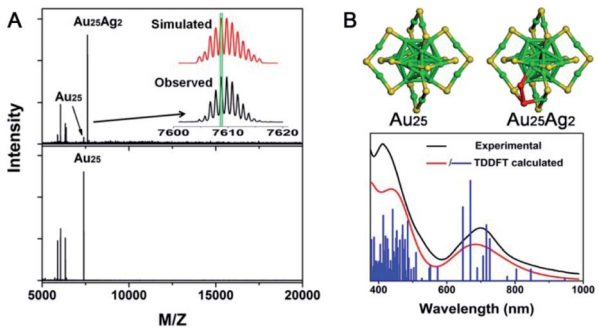

Fig. 17 (A) MALDI-MS spectra of $Au_{25}Ag_2$ and Au_{25}. (B) Structure of Au_{25} and $Au_{25}Ag_2$ and the comparison of the experimental and calculated spectra of $Au_{25}Ag_2$ (reproduced from ref. 103 with permission from the American Chemical Society, Copyright (2015)).

complex was exchanged, $Au_{24-x}Ag_xHg_1(PET)_{18}$ (x = 2–6) was obtained with a relatively low Ag content.[105]

3.4 Other methods and controlling parameters

Except for the abovementioned methods, there are also some other efficient approaches for synthesizing and controlling Au NCs, including oxidation/reduction-driven transformation, intercluster reactions, acid etching, and solvent induction, to name a few.

In the oxidation/reduction-driven method, the charge or even the structure of the parent NCs was often altered, and some examples are shown below. Early in 2008, Jin *et al.* reported the transformation from the $[Au_{25}(PET)_{18}]^-$ (Au_{25}^-) anionic cluster into a charge neutral cluster $[Au_{25}(PET)_{18}]^0$ (Au_{25}^0) *via* air oxidation or H_2O_2 oxidation.[106] Despite the similar structures, the staples of Au_{25}^0 have some apparent distortions; for instance, every two opposite $Au_2(SR)_3$ staples in Au_{25}^0 are completely coplanar with the symmetry plane of the icosahedron kernel. Negishi *et al.* studied the oxidation of hexanethiol-capped Au_{25} with the strong oxidizing agent $Ce(SO_4)_2$ and obtained positive Au_{25}.[107] In 2017, Jin and coworkers reported the structural transformation from another anionic Au NC ($Au_{23}(CHT)_{16}$) into $Au_{28}(CHT)_{20}$ by H_2O_2 oxidation.[108] Unlike the case of Au_{25}^- transformation to Au_{25}^0, the metal core and surface staples of Au_{28} are completely different from those of Au_{23}, indicating that oxidation-induced transformation is a potential method to access new structures of Au NCs. Wu *et al.* also found the conversion from $Au_{23}(CHT)_{16}$ to $Au_{28}(CHT)_{20}$ using $Cd(NO_3)_2$ as the oxidant.[92] Reduction-induced transformation has also been reported. For example, Jin and Zhu reported the transformation from $[Au_{25}(SePh)_{18}]^-$ to $[Au_{23}(SePh)_{16}]^-$ in the presence of reductive $NaBH_4$.[109] The direct loss of two Au–SR units in the parent Au_{25} was revealed by experiments and theoretical calculations.

Pradeep's group reported the first example of intercluster reactions between $Au_{25}(SR)_{18}$ and $Ag_{44}(SR)_{30}$ (SR: alkyl/aryl thiolate) (Fig. 18A).[110,111] The mass data demonstrated the exchange of the metal atoms as well as the metal–thiolate fragments. Of note, the number of Ag dopants added to Au_{25} could reach up to 20. The thermodynamic feasibility of the reaction has also been revealed using DFT calculations. Almost at the same time, inspired by AGR,[88,89] Wu *et al.* reported the reaction between hydrophilic metal nanoparticles (including nanoclusters) (Fig. 18B).[112] Captopril-protecting $Au_{25}(Capt)_{18}$ (Capt: Captopril) was chosen to react with $Ag_{30}(Capt)_{18}$, and a novel alloy NC ($Au_{20}Ag_5(Capt)_{18}$) was demonstrated by mass spectrometry and X-ray photoelectron spectroscopy. $Au_{20}Ag_5(Capt)_{18}$ showed enhanced photoluminescence with a quantum yield of *ca.* 7.6% relative to rhodamine 6G, which is 130 times and 38 times higher than that of $Au_{25}(Capt)_{18}$ or $Ag_{30}(Capt)_{18}$, respectively. Wu *et al.* further investigated the reaction between $Au_{25}(Capt)_{18}$ and silver (copper) nanoparticles and observed the mass peaks of Ag- or Cu-doped Au_{25}, indicating the universality of the interparticle reaction of water-soluble nanoparticles. In another example, Tsukuda *et al.* reported that the reaction between an equal amount of $[PtAu_{24}]^0$ and $[PtAu_{24}]^{2-}$ could produce two equivalents of $[PtAu_{24}]^-$, indicating possible electron transfer between differently valenced nanoclusters.[113]

Bulk gold is inert in common acids; however, nanoscale gold is not the same as bulk gold. Utilizing the activity of gold toward acid, Wu and coworkers introduced the acid-etching synthesis method and revealed the size-dependent reactivity of PET- and TBBT-capped gold nanoparticles with acetic acid:[114] large nanoparticles are still stable in acetic acid, while small nanoparticles (*e.g.*, Au_{25} and Au_{38}) show distinct reactivity with acetic acid. A new $Au_{38}(PET)_{26}$ nanocluster was obtained after etching Au_{25} in acetic acid overnight. $Au_{38}(PET)_{26}$ exhibited great disparities from the reported $Au_{38}(PET)_{24}$ in terms of both optical and electrochemical properties. The etching mechanism was also studied, and Wu *et al.* observed some intermediate species, such as $Au_n(PET)_{n+1}Cl_2(HAc)$ (n = 1–3, HAc: acetic acid), from mass spectra, indicating the possible attack of the staples by acetic acid.

More attention has been given to the structural transformation of Au NCs in solvents. Wei and coworkers reported an icosahedral-to-cuboctahedral structural transformation of Au_{13} driven by hexane.[115] The transformation process consists of the hexane-induced selective removal of the thiolate ligands from the Au_{13} surface, and the subsequent structure conversion process was monitored by X-ray absorption fine structure (XAFS) analyses. Xie *et al.* also reported the size-conversion reaction from $[Au_{23}(SR)_{16}]^-$ to $[Au_{25}(SR)_{18}]^-$ (SR: *para*-mercaptobenzoic acid) by changing the solvent polarity (*e.g.*, from water/ethanol to pure water).[116] A surface-motif-exchange-induced mechanism was revealed by tandem mass analyses. The Wu group recently found that one of the $Au_{28}(CHT)_{20}$ isomers (Au_{28i}) could be transformed into another (Au_{28ii}) in diverse solvents.[100] The dielectric-constant effect and deuteration effect were observed for the first time in the solvent-induced conversion process of Au NCs, which was also confirmed by the adsorption energies and free energies obtained from DFT calculations.

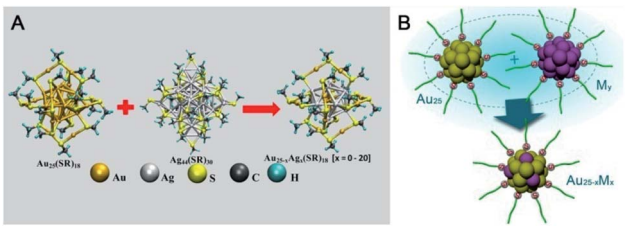

Fig. 18 (A) Intercluster reactions between $Au_{25}(SR)_{18}$ and $Ag_{44}(SR)_{30}$ (SR: alkyl/aryl thiolate) (reproduced from ref. 110 with permission from the American Chemical Society, Copyright (2016)). (B) The reaction between Au_{25} and Ag (Cu) nanoclusters or nanoparticles.

4. Summary and future outlook

The past two decades have witnessed the rapid development of the synthesis of Au NCs, undergoing the stages of the acquisition of Au NCs, the pursuit of monodispersity, structural determination, and controlling the composition and structure with atomic precision. In this review, we have introduced important research on controlling the synthesis of Au NCs by

categorizing the present synthetic methods into three main routes, (i) gold salt (complex) reduction, (ii) ligand induction, and (iii) antigalvanic reduction, noting the influences of various controlling parameters in the synthesis process. Although many types of Au NCs with diverse structures and compositions have been reported and explored, there are still several challenges for controlling Au NCs. At the end of this review, we attempt to propose several potential studies to address these issues:

(1) One to a few metal atom (ligand) manipulation. With the growing synthesis skill, we might expect the directed and precise removal, replacement or addition of one to a few metal atoms in NCs, with the remnant structures essentially being unchanged. Similarly, we also expect the manipulation of one to a few ligands (including reduction, addition and replacement) on the NC surface, with metal atom packing remaining untouched. Such a manipulation is of great significance not only for fundamental structure (composition)–property studies but also for improving the properties targeted for potential applications.

(2) Property-targeted control. Recently, Au NCs have attracted increasing attention due to their potential application in catalysis, sensing, and biology. Thus, the research community in this field is suggested to rationally control Au NCs with enhanced properties (*e.g.*, catalytic activity and fluorescence) based on the existing structure–property correlation.

(3) Development of doping methods. The precisely controlled synthesis of multi-metal (ligand) Au NCs is crucial for obtaining unique properties and practical applications due to the lower cost or newly imparted properties generated by foreign metal atoms (ligands) or synergistic effects. More metal elements, especially relatively active metals,[117] are expected to be doped into Au NCs. Controllable ligand doping has been rarely reported.

In brief, the future controlled synthesis of Au NCs will be developed not only with enriched sizes, compositions, and structures but also with attractive and selectable properties for applications.

Conflicts of interest

The authors have no conflicts of interest.

Acknowledgements

This work was supported by the National Natural Science Foundation of China (No. 21829501, 21701179, 21771186, 21925303, 21222301, 21603234, 21171170, and 21528303), Natural Science Foundation of Anhui Province (1708085QB36), CASHIPS Director's Fund (BJPY2019A02), Key Program of the 13th five year plan, CASHIPS (2020HSC-CIP005), and Innovative Program of Development Foundation of Hefei Center for Physical Science and Technology (2020HSC-CIP005) and CAS/SAFEA International Partnership Program for Creative Research Teams.

References

1 M. Haruta, *Chem. Rec.*, 2003, **3**, 75–87.
2 E. Boisselier and D. Astruc, *Chem. Soc. Rev.*, 2009, **38**, 1759–1782.
3 E. C. Dreaden, A. M. Alkilany, X. Huang, C. J. Murphy and M. A. El-Sayed, *Chem. Soc. Rev.*, 2012, **41**, 2740–2779.
4 M. Faraday, *Philos. Trans. R. Soc. London*, 1857, **147**, 145.
5 R. Ferrando, J. Jellinek and R. L. Johnston, *Chem. Rev.*, 2008, **108**, 845–910.
6 M. B. Cortie and A. M. McDonagh, *Chem. Rev.*, 2011, **111**, 3713–3735.
7 K. Saha, S. S. Agasti, C. Kim, X. Li and V. M. Rotello, *Chem. Rev.*, 2012, **112**, 2739–2779.
8 M. Grzelczak, J. Pérez-Juste, P. Mulvaney and L. M. Liz-Marzán, *Chem. Soc. Rev.*, 2008, **37**, 1783–1791.
9 Y. Xia, Y. Xiong, B. Lim and S. E. Skrabalak, *Angew. Chem., Int. Ed.*, 2009, **48**, 60–103.
10 T. Higaki, Q. Li, M. Zhou, S. Zhao, Y. Li, S. Li and R. Jin, *Acc. Chem. Res.*, 2018, **51**, 2764–2773.
11 R. Jin, C. Zeng, M. Zhou and Y. Chen, *Chem. Rev.*, 2016, **116**, 10346–10413.
12 I. Chakraborty and T. Pradeep, *Chem. Rev.*, 2017, **117**, 8208–8271.
13 H. Häkkinen, *Nat. Chem.*, 2012, **4**, 443–455.
14 A. Ghosh, O. F. Mohammed and O. M. Bakr, *Acc. Chem. Res.*, 2018, **51**, 3094–3103.
15 S. Hossain, Y. Niihori, L. V. Nair, B. Kumar, W. Kurashige and Y. Negishi, *Acc. Chem. Res.*, 2018, **51**, 3114–3124.
16 S. Wang, Q. Li, X. Kang and M. Zhu, *Acc. Chem. Res.*, 2018, **51**, 2784–2792.
17 J. Yan, B. K. Teo and N. Zheng, *Acc. Chem. Res.*, 2018, **51**, 3084–3093.
18 Q. Yao, X. Yuan, T. Chen, D. T. Leong and J. Xie, *Adv. Mater.*, 2018, **30**, 1870358.
19 R. P. Briñas, M. Hu, L. Qian, E. S. Lymar and J. F. Hainfeld, *J. Am. Chem. Soc.*, 2008, **130**, 975–982.
20 M. Zhu, E. Lanni, N. Garg, M. E. Bier and R. Jin, *J. Am. Chem. Soc.*, 2008, **130**, 1138–1139.
21 Z. Wu, J. Suhan and R. Jin, *J. Mater. Chem.*, 2009, **19**, 622–626.
22 H. Qian, Y. Zhu and R. Jin, *ACS Nano*, 2009, **3**, 3795–3803.
23 Z. Wu, M. A. MacDonald, J. Chen, P. Zhang and R. Jin, *J. Am. Chem. Soc.*, 2011, **133**, 9670–9673.
24 X. Yuan, B. Zhang, Z. Luo, Q. Yao, D. T. Leong, N. Yan and J. Xie, *Angew. Chem., Int. Ed.*, 2014, **53**, 4623–4627.
25 Z. Luo, V. Nachammai, B. Zhang, N. Yan, D. T. Leong, D.-e. Jiang and J. Xie, *J. Am. Chem. Soc.*, 2014, **136**, 10577–10580.
26 Y. Du, H. Sheng, D. Astruc and M. Zhu, *Chem. Rev.*, 2020, **120**, 526–622.
27 J. Fang, B. Zhang, Q. Yao, Y. Yang, J. Xie and N. Yan, *Coord. Chem. Rev.*, 2016, **322**, 1–29.
28 X. Yuan, X. Dou, K. Zheng and J. Xie, *Part. Part. Syst. Charact.*, 2015, **32**, 613–629.
29 M. Brust, M. Walker, D. Bethell, D. J. Schiffrin and R. Whyman, *J. Chem. Soc., Chem. Commun.*, 1994, 801–802.
30 A. Das, C. Liu, H. Y. Byun, K. Nobusada, S. Zhao, N. Rosi and R. Jin, *Angew. Chem., Int. Ed.*, 2015, **54**, 3140–3144.

31 A. Das, T. Li, K. Nobusada, C. Zeng, N. L. Rosi and R. Jin, *J. Am. Chem. Soc.*, 2013, **135**, 18264–18267.
32 M. W. Heaven, A. Dass, P. S. White, K. M. Holt and R. W. Murray, *J. Am. Chem. Soc.*, 2008, **130**, 3754–3755.
33 M. Zhu, C. M. Aikens, F. J. Hollander, G. C. Schatz and R. Jin, *J. Am. Chem. Soc.*, 2008, **130**, 5883–5885.
34 T. Higaki, C. Liu, C. Zeng, R. Jin, Y. Chen, N. L. Rosi and R. Jin, *Angew. Chem., Int. Ed.*, 2016, **55**, 6694–6697.
35 S. Zhuang, L. Liao, Y. Zhao, J. Yuan, C. Yao, X. Liu, J. Li, H. Deng, J. Yang and Z. Wu, *Chem. Sci.*, 2018, **9**, 2437–2442.
36 P. D. Jadzinsky, G. Calero, C. J. Ackerson, D. A. Bushnell and R. D. Kornberg, *Science*, 2007, **318**, 430–433.
37 H. Qian and R. Jin, *Nano Lett.*, 2009, **9**, 4083–4087.
38 N. Yan, N. Xia, L. Liao, M. Zhu, F. Jin, R. Jin and Z. Wu, *Sci. Adv.*, 2018, **4**, eaat7259.
39 L. C. McKenzie, T. O. Zaikova and J. E. Hutchison, *J. Am. Chem. Soc.*, 2014, **136**, 13426–13435.
40 X.-K. Wan, Z.-W. Lin and Q.-M. Wang, *J. Am. Chem. Soc.*, 2012, **134**, 14750–14752.
41 J. Chen, Q.-F. Zhang, T. A. Bonaccorso, P. G. Williard and L.-S. Wang, *J. Am. Chem. Soc.*, 2014, **136**, 92–95.
42 X.-K. Wan, Z.-J. Guan and Q.-M. Wang, *Angew. Chem., Int. Ed.*, 2017, **56**, 11494–11497.
43 Z. Gan, J. Chen, J. Wang, C. Wang, M. B. Li, C. Yao, S. Zhuang, A. Xu, L. Li and Z. Wu, *Nat. Commun.*, 2017, **8**, 14739.
44 Y. Shichibu, Y. Negishi, T. Watanabe, N. K. Chaki, H. Kawaguchi and T. Tsukuda, *J. Phys. Chem. C*, 2007, **111**, 7845–7847.
45 A. Das, T. Li, K. Nobusada, Q. Zeng, N. L. Rosi and R. Jin, *J. Am. Chem. Soc.*, 2012, **134**, 20286–20289.
46 X.-K. Wan, J.-Q. Wang, Z.-A. Nan and Q.-M. Wang, *Sci. Adv.*, 2017, **3**, e1701823.
47 C. Zeng, Y. Chen, K. Iida, K. Nobusada, K. Kirschbaum, K. J. Lambright and R. Jin, *J. Am. Chem. Soc.*, 2016, **138**, 3950–3953.
48 L. Liao, C. Yao, C. Wang, S. Tian, J. Chen, M.-B. Li, N. Xia, N. Yan and Z. Wu, *Anal. Chem.*, 2016, **88**, 11297–11301.
49 C. Zeng, Y. Chen, C. Liu, K. Nobusada, N. L. Rosi and R. Jin, *Sci. Adv.*, 2015, **1**, e1500425.
50 L. Liao, C. Wang, S. Zhuang, N. Yan, Y. Zhao, Y. Yang, J. Li, H. Deng and Z. Wu, *Angew. Chem., Int. Ed.*, 2020, **59**, 731–734.
51 L. Liao, J. Chen, C. Wang, S. Zhuang, N. Yan, C. Yao, N. Xia, L. Li, X. Bao and Z. Wu, *Chem. Commun.*, 2016, **52**, 12036–12039.
52 S. Zhuang, L. Liao, M.-B. Li, C. Yao, Y. Zhao, H. Dong, J. Li, H. Deng, L. Li and Z. Wu, *Nanoscale*, 2017, **9**, 14809–14813.
53 A. Tlahuice-Flores, R. L. Whetten and M. Jose-Yacaman, *J. Phys. Chem. C*, 2013, **117**, 20867–20875.
54 T. Chen, Q. Yao, X. Yuan, R. R. Nasaruddin and J. Xie, *J. Phys. Chem. C*, 2017, **121**, 10743–10751.
55 S. K. Katla, J. Zhang, E. Castro, R. A. Bernal and X. Li, *ACS Appl. Mater. Interfaces*, 2018, **10**, 75–82.
56 H. Qian and R. Jin, *Chem. Mater.*, 2011, **23**, 2209–2217.
57 S. Tian, Y.-Z. Li, M.-B. Li, J. Yuan, J. Yang, Z. Wu and R. Jin, *Nat. Commun.*, 2015, **6**, 8667.
58 Y. Yu, X. Chen, Q. Yao, Y. Yu, N. Yan and J. Xie, *Chem. Mater.*, 2013, **25**, 946–952.
59 Y. Yu, Z. Luo, D. M. Chevrier, D. T. Leong, P. Zhang, D.-e. Jiang and J. Xie, *J. Am. Chem. Soc.*, 2014, **136**, 1246–1249.
60 A. Ghosh, T. Udayabhaskararao and T. Pradeep, *J. Phys. Chem. Lett.*, 2012, **3**, 1997–2002.
61 F. Bertorelle, I. Russier-Antoine, C. Comby-Zerbino, F. Chirot, P. Dugourd, P.-F. Brevet and R. Antoine, *ACS Omega*, 2018, **3**, 15635–15642.
62 T. Chen, V. Fung, Q. Yao, Z. Luo, D.-e. Jiang and J. Xie, *J. Am. Chem. Soc.*, 2018, **140**, 11370–11377.
63 T. Chen, Q. Yao, Y. Cao and J. Xie, *Cell Rep. Phys. Sci.*, 2020, **1**, 100206.
64 S. Zhuang, L. Liao, J. Yuan, C. Wang, Y. Zhao, N. Xia, Z. Gan, W. Gu, J. Li, H. Deng, J. Yang and Z. Wu, *Angew. Chem., Int. Ed.*, 2018, **57**, 15450–15454.
65 S. Zhuang, L. Liao, J. Yuan, N. Xia, Y. Zhao, C. Wang, Z. Gan, N. Yan, L. He, J. Li, H. Deng, Z. Guan, J. Yang and Z. Wu, *Angew. Chem., Int. Ed.*, 2019, **58**, 4510–4514.
66 X. Meng, Z. Liu, M. Zhu and R. Jin, *Nanoscale Res. Lett.*, 2012, **7**, 277.
67 X. Zhu, S. Jin, S. Wang, X. Meng, C. Zhu, M. Zhu and R. Jin, *Chem.–Asian J.*, 2013, **8**, 2739–2745.
68 J. Yang, J. Y. Lee and J. Y. Ying, *Chem. Soc. Rev.*, 2011, **40**, 1672–1696.
69 G. H. Woehrle, L. O. Brown and J. E. Hutchison, *J. Am. Chem. Soc.*, 2005, **127**, 2172–2183.
70 Y. Shichibu, Y. Negishi, T. Watanabe, N. K. Chaki, H. Kawaguchi and T. Tsukuda, *J. Phys. Chem. C*, 2007, **111**, 7845–7847.
71 C. Zeng, Y. Chen, A. Das and R. Jin, *J. Phys. Chem. Lett.*, 2015, **6**, 2976–2986.
72 C. Zeng, C. Liu, Y. Pei and R. Jin, *ACS Nano*, 2013, **7**, 6138–6145.
73 C. Zeng, T. Li, A. Das, N. L. Rosi and R. Jin, *J. Am. Chem. Soc.*, 2013, **135**, 10011–10013.
74 Z. Gan, Y. Lin, L. Luo, G. Han, W. Liu, Z. Liu, C. Yao, L. Weng, L. Liao, J. Chen, X. Liu, Y. Luo, C. Wang, S. Wei and Z. Wu, *Angew. Chem., Int. Ed.*, 2016, **55**, 11567–11571.
75 P. R. Nimmala and A. Dass, *J. Am. Chem. Soc.*, 2014, **136**, 17016–17023.
76 C. Zeng, Y. Chen, K. Kirschbaum, K. Appavoo, M. Y. Sfeir and R. Jin, *Sci. Adv.*, 2015, **1**, e1500045.
77 Y. Chen, C. Zeng, D. R. Kauffman and R. Jin, *Nano Lett.*, 2015, **15**, 3603–3609.
78 Y. Chen, C. Zeng, C. Liu, K. Kirschbaum, C. Gayathri, R. R. Gil, N. L. Rosi and R. Jin, *J. Am. Chem. Soc.*, 2015, **137**, 10076–10079.
79 C. Zeng, Y. Chen, C. Liu, K. Nobusada, N. L. Rosi and R. Jin, *Sci. Adv.*, 2015, **1**, e1500425.
80 L. Liao, S. Zhuang, C. Yao, N. Yan, J. Chen, C. Wang, N. Xia, X. Liu, M.-B. Li, L. Li, X. Bao and Z. Wu, *J. Am. Chem. Soc.*, 2016, **138**, 10425–10428.
81 L. Liao, S. Zhuang, P. Wang, Y. Xu, N. Yan, H. Dong, C. Wang, Y. Zhao, N. Xia, J. Li, H. Deng, Y. Pei, S.-K. Tian and Z. Wu, *Angew. Chem., Int. Ed.*, 2017, **56**, 12644–12648.

82 H. Dong, L. Liao, S. Zhuang, C. Yao, J. Chen, S. Tian, M. Zhu, X. Liu, L. Li and Z. Wu, *Nanoscale*, 2017, **9**, 3742–3746.
83 P. Liu, W. Han, M. Zheng and W. W. Xu, *Nanoscale*, 2020, **12**, 20677–20683.
84 A. Tlahuice-Flores, *J. Phys. Chem. C*, 2019, **123**(17), 10831–10841.
85 A. Tlahuice-Flores, M. Jose-Yacamán and R. L. Whetten, *Phys. Chem. Chem. Phys.*, 2013, **15**, 19557–19560.
86 A. Tlahuice and I. L. Garzón, *Phys. Chem. Chem. Phys.*, 2012, **14**, 3737–3740.
87 W. W. Xu, X. C. Zeng and Y. Gao, *Acc. Chem. Res.*, 2018, **51**, 2739–2747.
88 Z. Wu, *Angew. Chem., Int. Ed.*, 2012, **51**, 2934–2938.
89 Z. Gan, N. Xia and Z. Wu, *Acc. Chem. Res.*, 2018, **51**, 2774–2783.
90 Z. Wu, M. Wang, J. Yang, X. Zheng, W. Cai, G. Meng, H. Qian, H. Wang and R. Jin, *Small*, 2012, **8**, 2028–2035.
91 S. Tian, C. Yao, L. Liao, N. Xia and Z. Wu, *Chem. Commun.*, 2015, **51**, 11773–11776.
92 Z. Min, W. Pu, Y. Nan, C. Xiaoqi, H. Lizhong, Z. Yan, X. Nan, Y. Chuanhao, L. Jin, D. Haiteng, Z. Yan, P. Yong and W. Zhikun, *Angew. Chem., Int. Ed.*, 2018, **57**, 4500–4504.
93 W. Zhang, S. Zhuang, L. Liao, H. Dong, N. Xia, J. Li, H. Deng and Z. Wu, *Inorg. Chem.*, 2019, **58**, 5388–5392.
94 S. Wang, L. Xiong, G. Sun, L. Tang, J. Zhang, Y. Pei and M. Zhu, *Nanoscale Adv.*, 2020, **2**, 664–668.
95 M.-B. Li, S.-K. Tian, Z. Wu and R. Jin, *Chem. Commun.*, 2015, **51**, 4433–4436.
96 S. Wang, Y. Song, S. Jin, X. Liu, J. Zhang, Y. Pei, X. Meng, M. Chen, P. Li and M. Zhu, *J. Am. Chem. Soc.*, 2015, **137**, 4018–4021.
97 C. Yao, Y.-J. Lin, J. Yuan, L. Liao, M. Zhu, L.-H. Weng, J. Yang and Z. Wu, *J. Am. Chem. Soc.*, 2015, **137**, 15350–15353.
98 M.-B. Li, S.-K. Tian and Z. Wu, *Chin. J. Chem.*, 2017, **35**, 567–571.
99 C. Yao, S. Tian, L. Liao, X. Liu, N. Xia, N. Yan, Z. Gan and Z. Wu, *Nanoscale*, 2015, **7**, 16200–16203.
100 N. Xia, J. Yuan, L. Liao, W. Zhang, J. Li, H. Deng, J. Yang and Z. Wu, *J. Am. Chem. Soc.*, 2020, **142**, 12140–12145.
101 F. Jin, H. Dong, Y. Zhao, S. Zhuang, L. Liao, N. Yan, W. Gu, J. Zha, J. Yuan, J. Li, H. Deng, Z. Gan, J. Yang and Z. Wu, *Acta Chim. Sin.*, 2020, **78**, 407–411.
102 S. Zhuang, D. Chen, L. Liao, Y. Zhao, N. Xia, W. Zhang, C. Wang, J. Yang and Z. Wu, *Angew. Chem., Int. Ed.*, 2020, **59**, 3073–3077.
103 C. Yao, J. Chen, M.-B. Li, L. Liu, J. Yang and Z. Wu, *Nano Lett.*, 2015, **15**, 1281–1287.
104 N. Yan, L. Liao, J. Yuan, Y.-J. Lin, L.-H. Weng, J. Yang and Z. Wu, *Chem. Mater.*, 2016, **28**, 8240–8247.
105 S. Yang, S. Wang, S. Jin, S. Chen, H. Sheng and M. Zhu, *Nanoscale*, 2015, **7**, 10005–10007.
106 M. Zhu, W. T. Eckenhoff, T. Pintauer and R. Jin, *J. Phys. Chem. C*, 2008, **112**, 14221–14224.
107 Y. Negishi, N. K. Chaki, Y. Shichibu, R. L. Whetten and T. Tsukuda, *J. Am. Chem. Soc.*, 2007, **129**, 11322–11323.
108 T. Higaki, C. Liu, Y. Chen, S. Zhao, C. Zeng, R. Jin, S. Wang, N. L. Rosi and R. Jin, *J. Phys. Chem. Lett.*, 2017, **8**, 866–870.
109 Y. Song, H. Abroshan, J. Chai, X. Kang, H. J. Kim, M. Zhu and R. Jin, *Chem. Mater.*, 2017, **29**, 3055–3061.
110 K. R. Krishnadas, A. Ghosh, A. Baksi, I. Chakraborty, G. Natarajan and T. Pradeep, *J. Am. Chem. Soc.*, 2016, **138**, 140–148.
111 K. R. Krishnadas, A. Baksi, A. Ghosh, G. Natarajan, A. Som and T. Pradeep, *Acc. Chem. Res.*, 2017, **50**, 1988–1996.
112 N. Xia and Z. Wu, *J. Mater. Chem. C*, 2016, **4**, 4125–4128.
113 M. Suyama, S. Takano, T. Nakamura and T. Tsukuda, *J. Am. Chem. Soc.*, 2019, **141**, 14048–14051.
114 N. Xia, Z. Gan, L. Liao, S. Zhuang and Z. Wu, *Chem. Commun.*, 2017, **53**, 11646–11649.
115 Y. Li, H. Cheng, T. Yao, Z. Sun, W. Yan, Y. Jiang, Y. Xie, Y. Sun, Y. Huang, S. Liu, J. Zhang, Y. Xie, T. Hu, L. Yang, Z. Wu and S. Wei, *J. Am. Chem. Soc.*, 2012, **134**, 17997–18003.
116 Q. Yao, V. Fung, C. Sun, S. Huang, T. Chen, D.-e. Jiang, J. Y. Lee and J. Xie, *Nat. Commun.*, 2018, **9**, 1979.
117 A. Tlahuice-Flores, *J. Nanopart. Res.*, 2013, **15**, 1771.